Structure and dynamics of the summertime atmospheric boundary layer over the Antarctic Plateau: 2. Heat, moisture, and momentum budgets

Dirk van As[1] and Michiel R. van den Broeke[1]

Received 6 December 2005; revised 6 December 2005; accepted 25 January 2006; published 4 April 2006.

[1] This paper presents the summertime budgets of heat, moisture and momentum in the atmospheric boundary layer at Kohnen base (75°00′S, 0°04′E, 2892 m above sea level), located in the interior of East Antarctica. For this purpose we performed a model simulation for clear-sky conditions and constant large-scale forcing, using a high-resolution one-dimensional atmospheric model which has been validated by observations (see van As et al., 2006). Turbulent exchange is the dominant component in the heat budget, heating the daytime well-mixed layer by a maximum of 1.0 K h^{-1}. Radiative heating and cooling are important, and are largest near the surface and just above and below the large temperature and humidity gradients of the nighttime stable layer. Vertical heat advection, which is introduced by the wind speed component along the slope, is the smallest heat-budget component in the atmospheric boundary layer, but becomes significant above it. The same is valid for vertical advection in the moisture budget, which is again dominated by turbulent exchange in the atmospheric boundary layer. The model generates solid precipitation (diamond dust) in the nighttime stable boundary layer. In the stable layer the temperature deficit with respect to the free atmosphere can be larger than 10 K, forcing a relatively large katabatic acceleration (up to 2.7 m s^{-1} h^{-1}). Katabatic forcing is chiefly opposed by turbulent momentum transfer (friction). The katabatic forcing decreases with height but is nonzero above the atmospheric boundary layer. In the nighttime stable layer we find a jet which is chiefly forced by katabatics, and in the residual layer above it we find alternating wind maxima and minima as a result of an inertial oscillation.

Citation: van As, D., and M. R. van den Broeke (2006), Structure and dynamics of the summertime atmospheric boundary layer over the Antarctic Plateau: 2. Heat, moisture, and momentum budgets, *J. Geophys. Res.*, *111*, D07103, doi:10.1029/2005JD006956.

1. Introduction

[2] Katabatic wind is a prominent aspect of the low-level Antarctic atmosphere [*Ball*, 1956; *Mather and Miller*, 1967; *Parish and Waight*, 1987]. This near-surface air flow arises when a sloping surface is cooled through a negative radiation budget. Turbulent heat exchange then cools the near-surface air and creates a stably stratified layer, i.e., a surface-based temperature inversion. The resulting horizontal pressure gradient generates down-slope katabatic winds, characterized by a distinctive near-surface wind maximum and a highly constant wind direction. *Brost and Wyngaard* [1978] showed that even gentle slopes of 1–10 m km^{-1} over a large area can cause a significant katabatic wind speed component. Katabatic forcing is believed to be the dominant force controlling the near-surface wind field over large parts of Antarctica [*van den Broeke and van Lipzig*, 2003]. However, it has been shown that jets in the lower troposphere over Antarctica can also be produced by other phenomena, such as mesoscale baroclinicity [*Kodama et al.*, 1989], and that a high directional constancy of the near-surface wind field can be caused by the predominant meridional pressure gradient over the continent [*Parish and Cassano*, 2003]. Detailed observations are necessary to unravel the various mechanisms active in forcing the Antarctic atmospheric boundary layer (ABL).

[3] Most observations of the structure and forcing of the Antarctic ABL [e.g., *Kottmeier*, 1986; *Sorbjan et al.*, 1986; *Heinemann*, 1988; *King*, 1989; *Kodama et al.*, 1989; *Bintanja*, 2000] are confined to the coastal and escarpment zones. An exception is *Mastrantonio et al.* [1999], who presented measurements of the summertime ABL at Dome C in the Antarctic interior, focusing the evolution of a mixed layer during daytime.

[4] The small amount of detailed observations has motivated a multitude of model-based studies of the katabatic ABL. *Heinemann* [1988] determined using a 1D model that at the Filchner/Ronne Ice Shelf front horizontal advection dominates the heat budget of the ABL. *King* [1989] was successful in reproducing observed wind profiles at the coastal Halley base, situated on a nearly flat ice shelf. *Parish et al.* [1993] applied a 2D model to the summertime ABL across Adélie Land and simulated the diurnal variation. The dynamics of the ABL at a coastal location near Neumayer station during a wintertime period were simulated by *Lykossov* [2001]. A 3D model simulation of the wintertime lower atmosphere over Coats Land and the fairly flat

[1]Institute for Marine and Atmospheric Research Utrecht, Utrecht University, Utrecht, Netherlands.

Copyright 2006 by the American Geophysical Union.
0148-0227/06/2005JD006956$09.00

Brunt Ice Shelf by *Renfrew* [2004] showed a jump from "shooting" to "tranquil" flow, which retreated in time from the ice shelf onto the continental slope.

[5] Three-dimensional atmospheric models were also applied to larger areas to study the Antarctic ABL, such as the model used by *Parish and Cassano* [2003] mentioned before. *van den Broeke et al.* [2002] presented the average modeled momentum budget of the Antarctic ABL. They confirmed for the surface layer that the mean katabatic force is smaller than the large-scale pressure gradient force in summer. In a follow-up paper, *van den Broeke and van Lipzig* [2003] showed great spatial variability in ABL forcings over the Antarctic continent.

[6] To gain more insight in the summertime ABL on the Antarctic Plateau, the EPICA-Netherlands Atmospheric Boundary Layer Experiment (ENABLE) was performed at Kohnen base (75°00′S, 0°04′E, 2892 m above sea level) in January and February 2002 [*van As et al.*, 2006] (hereinafter referred to as part 1). At this location the snow surface slopes up by 1.3 ± 0.3 m km^{-1} in east-north-easterly direction (61 ± 15°). The surface energy budget during ENABLE was presented by *van As et al.* [2005a].

[7] This paper describes a model study of the summertime clear-sky ABL at Kohnen. It follows up on part 1, which validated a one-dimensional model to the ENABLE location and period. Here we present the heat, moisture and momentum balances of the ABL.

[8] This paper is organized as follows. After a model presentation in section 2, the ABL structure and dynamics and the heat, moisture and momentum budgets are presented in section 3. A discussion follows in section 4 and a summary is given in section 5.

2. Methods

2.1. Model Description

[9] As the length scale at which the surface slope changes at the Antarctic Plateau is much larger than the vertical extent of our model, one dimension suffices to simulate the ABL over the plateau. The model, originally developed by *Duynkerke* [1991], uses two hundred vertical levels with a nonlinear grid spacing ranging from 1.6 × 10^{-2} m at the surface to 18 m at 2000 m altitude. The model has been adapted for Antarctic conditions to describe the ABL over a highly reflective and smooth sloping surface without vegetation.

[10] The following conservation equations of heat, moisture and momentum are solved on a tilted grid where the y axis points in down-slope direction and z is perpendicular to the surface:

$$\begin{aligned}
\underset{STO}{\frac{\partial \theta}{\partial t}} &= \underset{VAD}{-v\gamma_\theta B_\theta \sin\beta} \quad \underset{TUR}{-\frac{\partial \overline{w'\theta'}}{\partial z}} \quad \underset{RAD,}{-\frac{1}{\rho c_p}\frac{\partial R_{net}}{\partial z}} \\
\underset{STO}{\frac{\partial q}{\partial t}} &= \underset{VAD}{-v\gamma_q B_q \sin\beta} \quad \underset{TUR}{-\frac{\partial \overline{w'q'}}{\partial z}} \quad \underset{PRE,}{-Q} \\
\underset{STO}{\frac{\partial u}{\partial t}} &= \underset{COR+LSC}{f(v - v_g)} \quad \underset{TUR,}{-\frac{\partial \overline{u'w'}}{\partial z}} \\
\underset{STO}{\frac{\partial v}{\partial t}} &= \underset{COR+LSC}{-f(u - u_g)\cos\beta} \quad \underset{TUR}{-\frac{\partial \overline{v'w'}}{\partial z}} \quad \underset{KAT,}{-g\frac{\theta - \theta_0}{\theta_0}\sin\beta}
\end{aligned} \tag{1}$$

where

θ	potential temperature;
q	specific humidity;
$u/v/w$	wind speed in x/y/z direction;
u_g/v_g	geostrophic wind speed components;
x/y	cross-slope/along-slope coordinate;
z	coordinate perpendicular to the surface;
t	time;
$\gamma_{\theta/q}$	free-atmospheric lapse rate of θ/q;
$B_{\theta/q}$	θ/q plane tilt parameter;
$\sin\beta$	surface slope;
ρ	air density;
c_p	heat capacity of dry air; (assumed constant at 1005 J K^{-1} kg^{-1});
R_{net}	net radiation flux;
Q	precipitation;
f	Coriolis parameter (−1.41 × 10^{-4} s^{-1});
g	gravitational acceleration; (9.81 m s^{-2});
θ_0	background potential temperature.

Primes indicate perturbations. The multiplication factor cos β arises from the tilted coordinate system.

[11] The lower boundary condition for the heat budget is surface temperature, which is found by solving the surface energy balance (SEB). For a nonmelting, infinitely thin surface layer without heat capacity the SEB is

$$R_{net} + H_S + H_L + G = 0. \tag{2}$$

Here H_S and H_L are the surface-layer sensible and latent heat fluxes, respectively, which are calculated in accordance with Monin-Obukhov similarity theory [*Nieuwstadt*, 1984]. G is the subsurface heat flux, using the heat flux parameterization for a homogeneous slab of soil by *Deardorff* [1978]. The surface fluxes are defined positive when directed toward the surface.

[12] The individual terms in equation (1) are named as follows:

STO	storage/tendency;
VAD	vertical advection;
TUR	turbulent diffusion;
RAD	radiation divergence;
PRE	moisture sink by precipitation;
COR	Coriolis forcing;
LSC	large-scale forcing;
KAT	katabatic forcing.

These represent the sinks and sources for heat, moisture and momentum in the ABL. STO is the sum of all forcings and gives the tendency in heat, moisture content or wind speed. VAD is the only remaining advection term in the conservation equations as we assume cross-slope homogeneity and no mean wind speed component perpendicular to the surface in our tilted coordinate system. Even though VAD is the rewritten advection term in y direction for a horizontal ABL, we name it "vertical" advection as the term describes the along-slope transport of heat and moisture from higher/lower atmospheric levels. We added the parameters B_θ and B_q, which are a measure for the slope of the free-atmospheric θ and q isolines relative to the surface (B = 0 for isolines parallel to the surface, for horizontal θ and q planes B equals unity. Since potential temperature in the free

Table 1. Model Constants and Initial Variable Values

Parameter	Value
Surface slope (sin β)	1.3 m km^{-1}
Surface albedo	0.85
Surface pressure	670 hPa
T lapse rate (γ_T)	-5.0 K km^{-1}
Extrapolated surface T	247 K
θ plane tilt parameter (B_θ)	0.5
q lapse rate (γ_q)	-0.13×10^{-6} m^{-1}
Extrapolated surface q	0.36 g kg^{-1}
q plane tilt parameter (B_q)	0.3
Geostrophic wind speed (U_g)	4.5 m s^{-1}
Geostrophic wind direction	61° (downslope)
Soil/snow density	350 kg m^{-3}
Initial snow T	240 K

atmosphere increases with height while specific humidity generally decreases, down-slope advected air is relatively warm and dry. Pure horizontal advection is not taken into account, which is a reasonable assumption for a fair-weather period over the horizontally very homogeneous Antarctic snow surface.

[13] The vertical gradients of the kinematic turbulent fluxes give TUR; a positive gradient indicates downward turbulent transfer. For the turbulence calculation a first-order closure is used, in which the turbulent transfer coefficient for momentum/heat and moisture is defined as

$$K_{m/h} = l^2 \left(\left(\frac{\partial u}{\partial z} \right)^2 + \left(\frac{\partial v}{\partial z} \right)^2 \right)^{1/2} \left(\phi_m \, \phi_{m/h} \right)^{-1}, \qquad (3)$$

where the mixing length $l = \kappa z$, and $\kappa = 0.4$ is Von Kármán's constant. The stability-correction functions ϕ by *Duynkerke* [1991] were used for stable stratification, and those by *Dyer* [1974] for unstable stratification. Similar closures have been successfully applied over Antarctica by, for example, *King* [1989] and *van Lipzig et al.* [2004].

[14] The turbulent and radiative fluxes in equation (1) are defined perpendicular to the surface, and are positive when pointed away from the surface, in contrast to the surface fluxes in equation (2).

[15] Saturation leads to the formation of clear-sky precipitation (PRE) in the model. This falls to the surface without interaction with radiation, which is justified given the very small amount of precipitation produced by the model. The amount of precipitation is likely to be a slight overestimate as supersaturation is not allowed in the model, but is known to occur in Antarctica [*King and Anderson*, 1999]. Sublimation of solid precipitation in a layer of unsaturated air is not taken into account. The latent heat that is produced during the formation of the ice crystals in our simulation would cause a maximum temperature change of about 0.03 K h^{-1}. This is a small heating rate compared to the temperature changes in the ABL which are up to 30 times larger and can be neglected.

[16] KAT represents the negative buoyancy of cooled air over a sloping surface, and depends linearly on both surface slope and the temperature deficit ($\theta - \theta_0$). Here θ_0 is the downward extrapolated free-atmospheric potential temperature. In the stably stratified boundary layer, the temperature deficit and thus KAT are largest at the surface. We assume that θ_0 is constant in time. In this setup the model can only be run over a limited amount of time as θ_0 might gradually become less representable for the actual free-atmospheric temperature.

[17] We have neglected large-scale subsidence, which may arise from the divergence in the katabatic wind field over Antarctica. From European Centre for Medium-range Weather Forecast reanalysis data (ERA-40), we estimate that large-scale subsidence over Kohnen in the summer is in the order of 1 mm s^{-1}. For our model simulation this implies a heating of less than 0.02 K h^{-1}, which has little effect on ABL structure and dynamics. The assumptions made in the model are justified by the good agreement between the observations and model results (see part 1).

2.2. Model Simulation

[18] For the model simulation we selected a 4-day period at the end of the Antarctic summer (31 January to 3 February 2002) at the location of Kohnen base. The model was run for 5 days in total. The first day served as model spinup time, during which the model created a realistic initial boundary layer. Local time is equal to GMT owing to the longitude of Kohnen at 0°04′E.

[19] During the simulation period no clouds or strong large-scale horizontal advection were observed at Kohnen. Fair-weather conditions are common on the Antarctic Plateau as the escarpment region of the continent functions as a barrier for synoptic disturbances. We have determined from AWS observations that clear-sky conditions dominate at Kohnen; cloud fractions below 40% occur an estimated 70% of the time throughout the year.

[20] Table 1 lists the most important model parameters [see also *van As et al.*, 2005a]. None of the parameters has been tuned to fit observations. B_θ and B_q were determined from ERA-40 data. Initial values of temperature (T), specific humidity (q), wind speed (U) and direction (d) were chosen on the basis of measurements by tethersonde and radiosonde during the ENABLE campaign. The geostrophic/large-scale wind speed (U_g) is chosen to be constant with height and in time; this simplification facilitates the interpretation of the model output. Tethersonde observations during the 4-day simulation period show that U_g was in fact not constant, but varied between 2 and 7 m s^{-1}. The free-atmospheric wind direction was mostly directed downslope, which is common for this location owing to the easterly large-scale wind over Antarctica. In the simulation we aligned the large-scale wind with the fall line of the surface (so $v_g = U_g$). In a future publication we will investigate the sensitivity of the Antarctic ABL to changes in large-scale wind speed and direction.

[21] The model results have been validated by observations of temperature, humidity, wind speed and direction, and SEB components obtained at Kohnen base. Agreement between the observations and model results was good (see part 1). Differences were mainly found for the humidity profiles, likely owing to sensor inaccuracies of tether- and radiosonde. Also, the model underestimated near-surface wind shear in stable stratification, which can be related to our choice of the stability-correction function for momentum at low stability. Finally, the model produced an inertial oscillation in the residual layer at night which was not

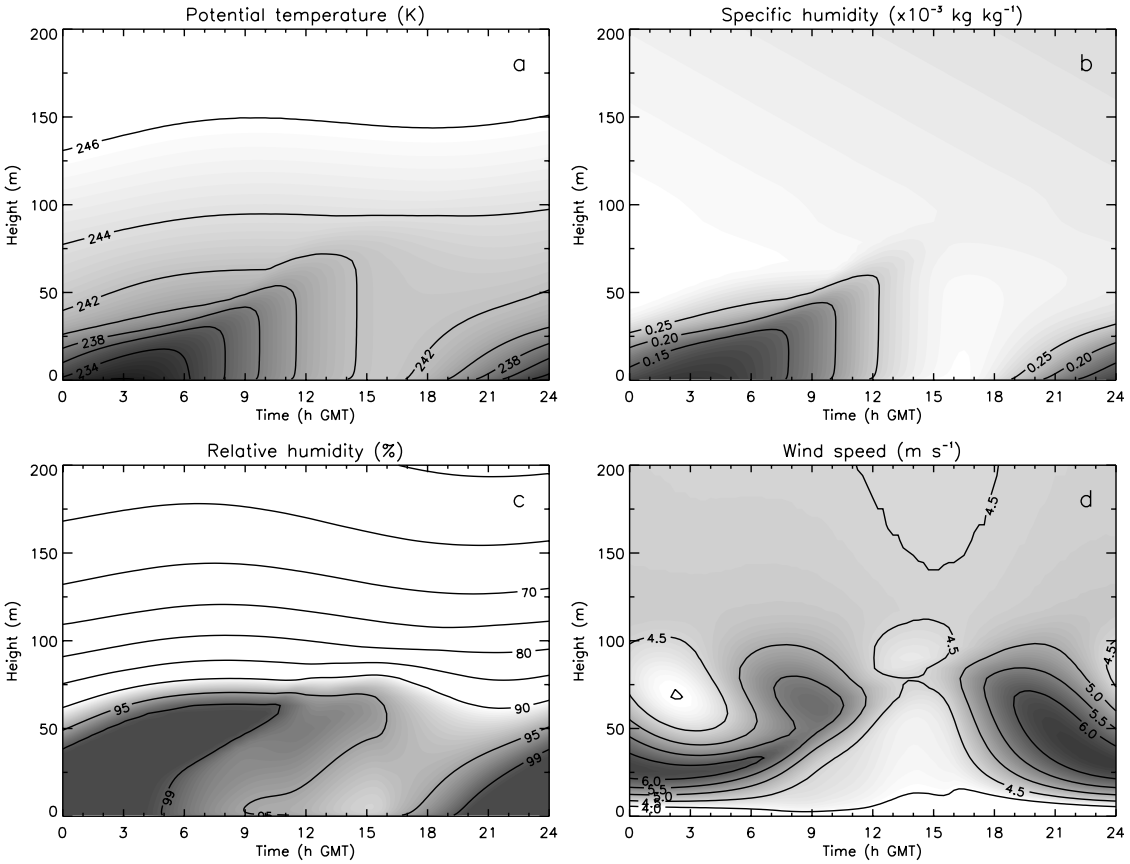

Figure 1. Mean modeled (a) potential temperature, (b) specific humidity, (c) relative humidity, and (d) wind speed.

clearly observed. The inertial oscillation will be further discussed in this paper.

3. Results

3.1. Temperature, Moisture, and Wind

[22] During summertime fair-weather conditions, R_{net} is positive at the surface during the day (energy is added to the surface) in spite of longwave radiative cooling, and is negative at night. This causes a strong daily cycle in surface temperature [*van As et al.*, 2005b] and therewith influences the structure and dynamics of the ABL.

[23] Figure 1 shows the mean daily cycle of simulated θ, q, relative humidity (RH) (with respect to ice) and U. During the day we find an unstably stratified surface layer with above it a mixed layer that increases its depth in time

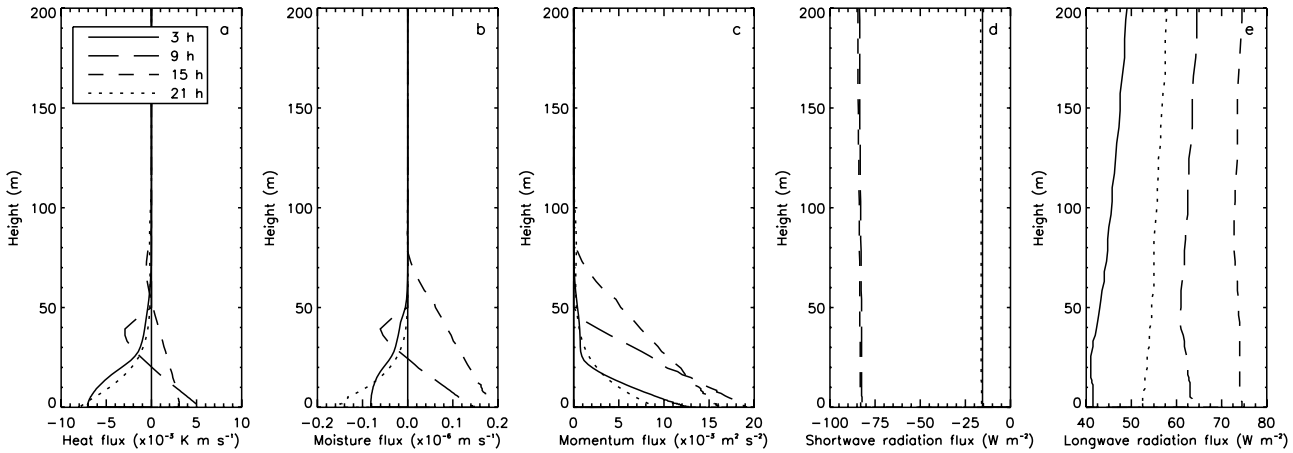

Figure 2. Mean modeled vertical fluxes of (a) heat, (b) moisture, (c) momentum ($=((\overline{u'w'})^2 + (\overline{v'w'})^2)^{0.5}$), (d) net shortwave radiation, and (e) net longwave radiation at 0300, 0900, 1500, and 2100 GMT. The fluxes in Figures 2a, 2b, 2d, and 2e are positive when directed away from the surface.

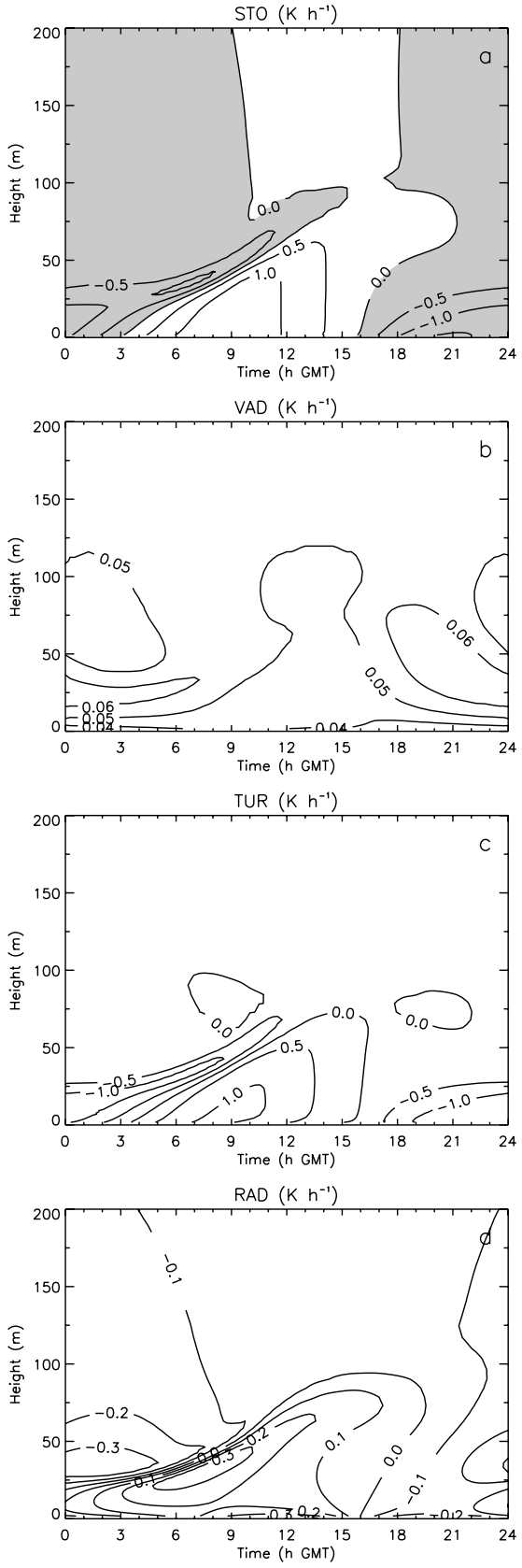

Figure 3. Mean modeled heat budget components: (a) storage, (b) vertical advection, (c) turbulent diffusion, and (d) radiation divergence.

(Figure 1a). During the night an increasingly deep stably stratified layer forms with a maximum temperature deficit (with respect to the free atmosphere) of over 10 K. Above this layer is the residual layer, which is the near-neutral remainder of the daytime mixed layer. The vertical extent of the ABL is limited to approximately 80 m.

[24] Specific humidity (Figure 1b) follows temperature owing to the strong dependence of saturation vapor pressure on temperature and the fact that RH in the ABL is always near saturation (Figure 1c), which is common over snow and ice surfaces [*Andreas et al.*, 2002]. A minimum RH value of 93% is attained in the mixed layer at 1500 GMT. Saturation occurs in the stably stratified part of the ABL between 2000 GMT in the evening and 1000 GMT in the morning. Above the ABL we find a small decrease in q with time due to vertical advection of dry air.

[25] In the daytime mixed layer a fairly uniform wind speed is found throughout the ABL (Figure 1d). However, from 1600 GMT onward an acceleration takes place in a large part of the ABL and a low-level jet is formed. During the evening the height of the jet is reduced from 80 m to 30 m. At night, the wind speed profile is reasonably constant in time and a wind speed minimum is present above the low-level jet, at around 70 m height. In the morning the jet grows weaker and rises to about 70 m height at 0900 GMT. Owing to the presence of a surface slope at Kohnen this jet is at least partially katabatic in the temperature-deficit layer. However, because the jet is initiated outside of the stably stratified layer, where we find alternating wind speed minima and maxima, we speculate that the jet is not is not entirely katabatic in nature, and might be partially forced by an inertial oscillation. We will look into this in section 3.5.

3.2. Flux Profiles

[26] Figure 2 shows the vertical turbulent fluxes of heat, moisture and momentum and vertical fluxes of net shortwave (SR_{net}) and longwave radiation (LR_{net}) at 0300, 0900, 1500 and 2100 GMT. These times were chosen to coincide with the minimum and maximum near-surface temperatures at 0300 and 1500 GMT, respectively, and with the moments of largest near-surface temperature change at 0900 and 2100 GMT.

[27] Turbulence transports heat and moisture downward at 2100 and 0300 GMT (Figures 2a and 2b). At 0900 GMT, temperature and specific humidity in the mixed layer increase owing to both surface fluxes (<40 m) and entrainment fluxes (40–50 m) of T and q. At the end of the unstable period at 1500 GMT the heat entrainment flux is small owing to a small inversion at the top of the ABL. There is no moisture entrainment at 1500 GMT as the gradient in q at the top of the ABL has disappeared.

[28] The vertical momentum flux ($= ((\overline{u'w'})^2 + (\overline{v'w'})^2)^{0.5}$) is large near the surface and decreases with height at all times (Figure 2c). In the mixed layer at 0900 and 1500 GMT the surface is a larger sink for momentum than during stable stratification. Above the nocturnal jet the momentum flux increases slightly with height. Here the negative wind shear causes an upward, but very small transport of momentum.

[29] The vertical profiles of SR_{net} and LR_{net} in Figures 2d and 2e show that radiative heating is chiefly the result of LR

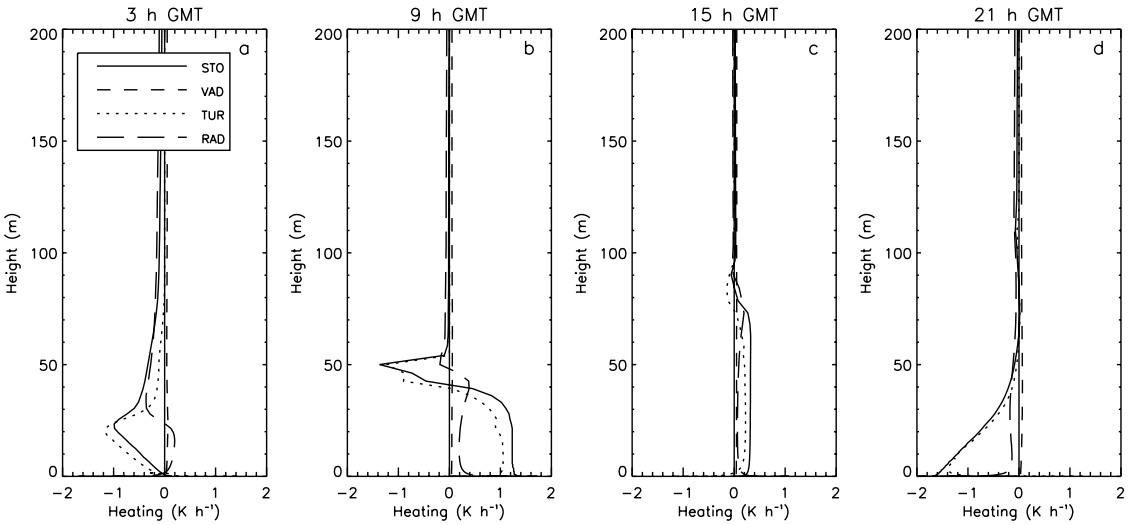

Figure 4. Mean modeled heat budget components at (a) 0300, (b) 0900, (c) 1500, and (d) 2100 GMT.

divergence. In the figures SR_{net} is negative and LR_{net} is positive as fluxes are defined positive when directed upward. SR_{net} exhibits no large divergence for clear skies. Above the ABL, the generally increasing LR with height cools the atmosphere (Figure 2e). This cooling is smallest in the afternoon, when the emission of radiation from the surface peaks. Inside the ABL, negative gradients in LR occur, especially in the stably stratified air, implying radiative heating. LR divergence in the ABL is smallest at 1500 GMT. At 2100 GMT the entire simulated air column is cooled by radiation.

3.3. Heat Budget

[30] Figure 3 shows the ABL heat-budget components, defined in equation (1). Figure 3a shows the heating of the mixed layer during daytime, which continues in the residual layer up to 2100 GMT. Hereafter a cooling of up to 1.2 K h^{-1} occurs, which is strongest near the surface in the evening. After midnight, near-surface cooling changes to warming around 0300 GMT, 4 hours before H_S changes sign and a mixed layer is formed. However, cooling continues during the morning and part of the afternoon in a thin layer of air approximately 20 m deep, at increasing elevation.

[31] The contribution of vertical advection to the heat budget of the ABL is small (Figure 3b) and its variability is fully determined by the along-slope wind speed (see equation (1)). The figure shows that advective heating is always positive, which indicates that there is always a down-slope wind component.

[32] The turbulent term is the dominant heat-budget component in the ABL (Figure 3c). During night, large wind shear causes strong mechanical turbulence and thereby transporting relatively cool air upward and warm air downward. Whether the air warms or cools by this process chiefly depends on the capacity of the surface to cool through a negative radiation budget. From 0200–0300 GMT onward, surface temperature rises and the surface radiation budget becomes less negative owing to the increasing solar elevation. The onset of heating of near-surface air by turbulent transport occurs an hour later. While TUR starts to heat the ABL from below in the morning, it cools the air higher in the ABL, driven by the wind shear of the low-level jet. Values of TUR are positive in the entire mixed layer until it can no longer be sustained by H_S around 15 h GMT.

[33] Longwave-radiation divergence constitutes a significant term in the ABL heat budget and is largest nearby large gradients in temperature and humidity in the ABL (Figure 3d). These gradients occur in the temperature-deficit layer at night and in the morning, and in the surface layer around noon and in the evening. The residual layer is largely cooled by RAD, while the mixed layer is heated.

[34] Figure 4 offers a better view on the relative importance of the heat budget components at 0300, 090, 1500 and 2100 GMT. The figures show the ever positive and small contribution of VAD (short dashes) to the heat budget, which is only significant above the ABL where it is opposed by radiative cooling (long dashes). TUR (dotted line) contributes most to temperature changes in the lower ABL at all times. However, RAD is an almost equally important term at the top of both the stable and mixed layer, and in the surface layer.

3.4. Moisture Budget

[35] Figure 5a shows the temporal rate of change in moisture content of the ABL. The moisture tendency is positive in the mixed layer and negative in the evening and night, but absolute changes in moisture content are small.

[36] The largest contributor to the moisture budget in the ABL is again turbulent diffusion (Figure 5c). TUR chiefly distributes the moisture over the ABL that is gained at the surface during daytime (Figure 2b) and transports moisture toward the surface at night. Moisture content change due to turbulent diffusion ranges from less than -2×10^{-5} kg kg^{-1} h^{-1} in the lowest 20 m of the ABL in the evening to over $+2 \times 10^{-5}$ kg kg^{-1} h^{-1} in the lowest 50 m of the ABL in the late morning.

[37] Vertical advection of moisture (Figure 5b) is relatively small. Where VAD is a positive contribution to the heat budget (Figure 3b), it is negative for the moisture budget, because the gradients of the free-atmospheric pro-

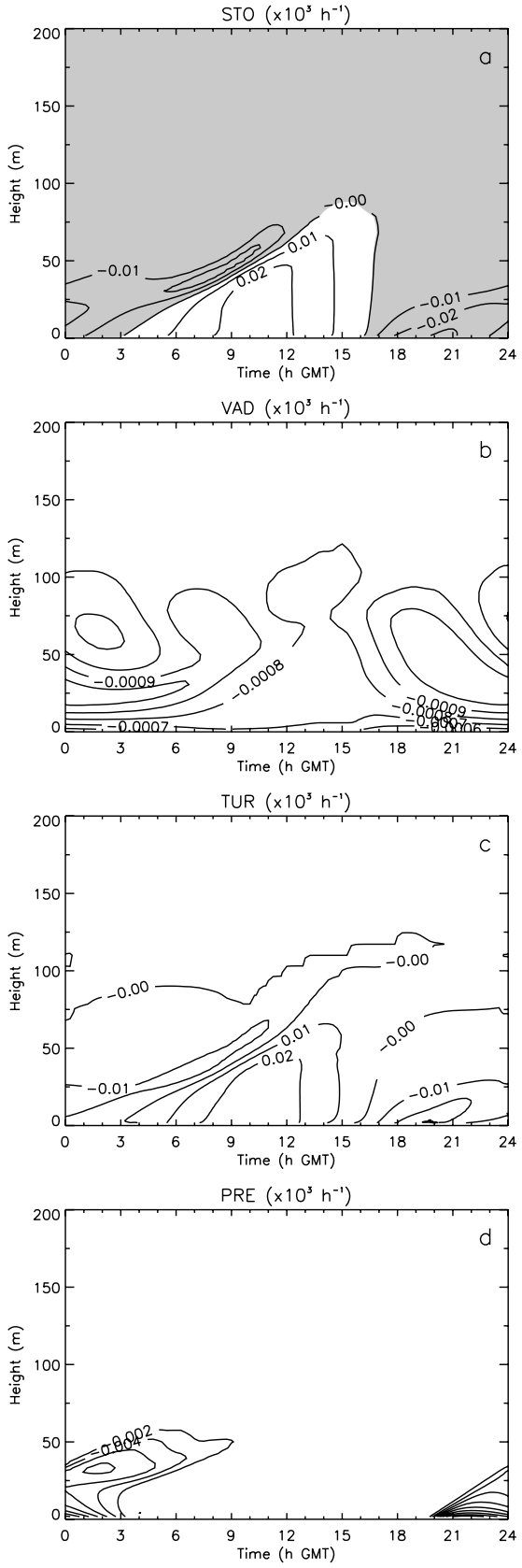

Figure 5. Mean modeled moisture budget components: (a) storage, (b) vertical advection, (c) turbulent diffusion, and (d) precipitation in g kg^{-1} h^{-1}.

files of θ and q are of opposite sign. Above the ABL, VAD is the main component in the moisture budget and causes the decrease in q that was observed in Figure 1b.

[38] Saturation occurs in the cooling ABL during the evening and night. In the model this leads to the formation of a small amount of solid precipitation (Figure 5d). Precipitation formation starts at the surface at 2000 GMT; the layer of solid precipitation production increases in depth in the following hours. From 0400 GMT precipitation formation ceases near the surface, but continues in the higher part of the ABL.

[39] The profiles of the moisture budget components in Figure 6 show that moisture loss by solid precipitation formation (dashed line) is significant in the lower part of the ABL at 2100 GMT and between 30 and 50 m height at 0300 GMT. The figure also shows slightly positive values for TUR at the surface at 0300 GMT (in contrast to TUR of heat), which is opposed by precipitation formation, resulting in $\partial q/\partial t = 0$. During the day, turbulent diffusion (dotted line) is the only significant mechanism for moisture change.

[40] The model predicts 2.1×10^{-3} mm water equivalent of ice crystals to precipitate on the surface per day. In comparison, during the evening and night, 4.7×10^{-3} mm water equivalent is deposited at the surface owing to a positive H_L. Daily mean H_L has a negative value of -1.2×10^{-1} W m^{-2}, which translates into a net sublimation of 3.6×10^{-3} mm water equivalent per day. This net transport of moisture from the surface to the ABL compensates for the moisture loss through entrainment and vertical advection of relatively dry air.

3.5. Momentum Budget

[41] We only present the momentum budget in the along-slope direction; in the cross-slope direction a simple geostrophic balance between Coriolis and large-scale forcing is found. Momentum storage and turbulent diffusion in cross-slope direction are relatively small as ABL wind speed is largest in along-slope direction.

[42] Figure 7 shows the mean daily cycle of the momentum-budget components in the down-slope direction. Equation (1) shows that the along-slope acceleration (Figure 7a) has four components (COR, LSC, TUR and KAT), of which the large-scale forcing is zero in this case since the cross-slope component of the large-scale wind speed $u_g = 0$. The variability in the Coriolis acceleration in Figure 7b is a measure for the strength of the cross-slope wind speed and is largest in the nighttime low-level jet.

[43] The turbulent friction term (Figure 7c) is chiefly negative. The largest turbulent deceleration occurs near the surface at night when the wind shear is large. During daytime the mixed layer is more uniformly decelerated. In regions above the jet, TUR has slightly positive values.

[44] Figure 7d shows that the katabatic term is always positive. The continuous radiative cooling of the lowest few hundred meters of the free atmosphere (Figure 4d), in combination with a constant temperature-background state (θ_0), makes that the katabatic forcing is not confined to the ABL but extends toward higher levels. In spite of the small surface slope, the large temperature deficit at night causes a katabatic acceleration of over 2.6 m s^{-1} h^{-1}. Even the mixed layer during the day is katabatically accelerated by

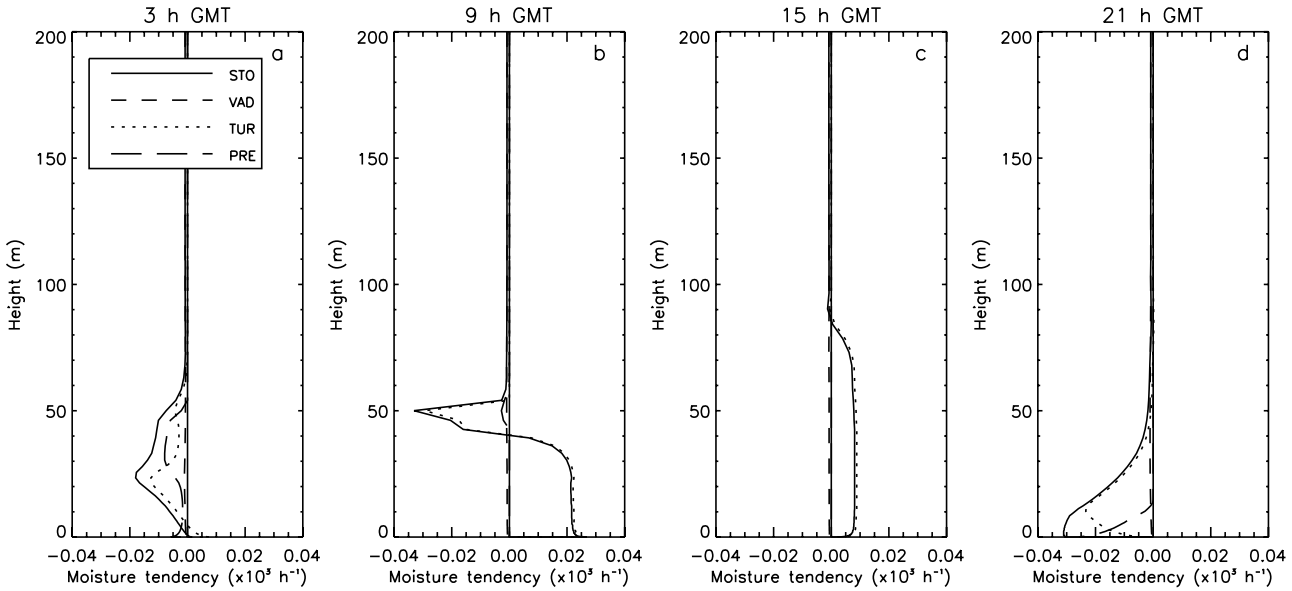

Figure 6. Mean modeled moisture budget components at (a) 0300, (b) 0900, (c) 1500, and (d) 2100 GMT in g kg^{-1} h^{-1}.

1.0 m s^{-1} h^{-1}, which prevents the formation of anabatic (up-slope) winds.

[45] The temporal wind speed variability in along-slope direction is given in Figure 7a. The daily cycle of along-slope wind depends strongly on its vertical level: Near the surface (up to 10 m) we find increasing wind speed during the evening, night and part of the morning, implying a near-surface wind maximum between 0800 and 0900 GMT. For a brief period after midnight no acceleration of the nocturnal jet takes place. During daytime, from 0900 GMT onward, the mixed layer is decelerating. In the residual layer, between 50 and 100 m height at night, we find periodical wind speed variations. This is the manifestation of an inertial oscillation, which is triggered by a sudden stabilization of near-surface air and the associated reduction in friction in the afternoon (Figure 7c).

[46] Figure 8 also reveals the alternating acceleration and deceleration in the residual layer (solid line) where TUR is small or absent (dotted line). Turbulence mainly opposes the katabatic forcing (long dashes) in the near-surface air. Within the temperature-deficit layer KAT dominates the momentum balance. Katabatic forcing is still present at 200 m height, above the ABL, where it is balanced by Coriolis forcing. This nonzero along-slope Coriolis term causes a rotation of the wind vector.

4. Discussion

[47] Figure 9 shows the wind direction during the simulation period at four atmospheric levels. These levels were chosen in the surface layer (long dashes), at the approximate height of the katabatic jet (short dashes), at the height of the inertial oscillation (dotted line) and outside of the ABL and temperature-deficit layer (solid line). The mass transport at these levels does not deviate more than 33° from the fall line. In the mixed layer, wind directions at 2 and 20 m are identical. As the mixed layer deepens and slows down, 70-m winds are forced in the same direction. During the evening and night Coriolis forces the katabatic airflow slightly to the left. At 70 m height the inertial oscillation is clearly visible.

[48] Figure 10 shows the mean daily cycle of the wind vector at 70 m height. Between 1000 and 1100 GMT, turbulent diffusion becomes significant at 70 m height (Figure 7c), from which moment the wind vector moves toward the geostrophic wind vector. A new oscillation is initiated when friction drops rapidly at 1500 GMT. The rotation of the wind vector during the night describes a damped oscillation as friction remains nonzero owing to significant wind shear above the nocturnal katabatic jet. Super-geostrophic wind speeds are found between 0500 and 1200 GMT and between 1600 GMT and midnight. Wind vectors for 0000 and 2400 GMT are not identical, indicating that katabatic forcing has increased over the simulated 4-day period owing to a gradual cooling of the ABL. During the entire day the wind at 70 m height is directed more to the left than the large-scale wind. This will be discussed below.

[49] Figure 7c shows that the inertial oscillation is initiated when the CBL collapses in the afternoon. Without friction the momentum balance over a horizontal surface is reduced to a balance between storage, the Coriolis force, and the large-scale pressure-gradient force,

$$\frac{\partial u}{\partial t} = f\left(v - v_g\right), \qquad \frac{\partial v}{\partial t} = -f\left(u - u_g\right), \tag{4}$$

The solution of these equations is an oscillation about the geostrophic wind vector (u_g,v_g), provided that (u,v) $\neq$ (u_g,v_g) [*Blackadar*, 1957].

[50] Compared to midlatitudes, two important differences exist with the oscillation found over the Antarctic Plateau. First, owing to the high latitude the oscillation period is shorter than at midlatitudes; at Kohnen the oscillation period is 12.4 hours, compared to 16.9 hours at 45°S. This

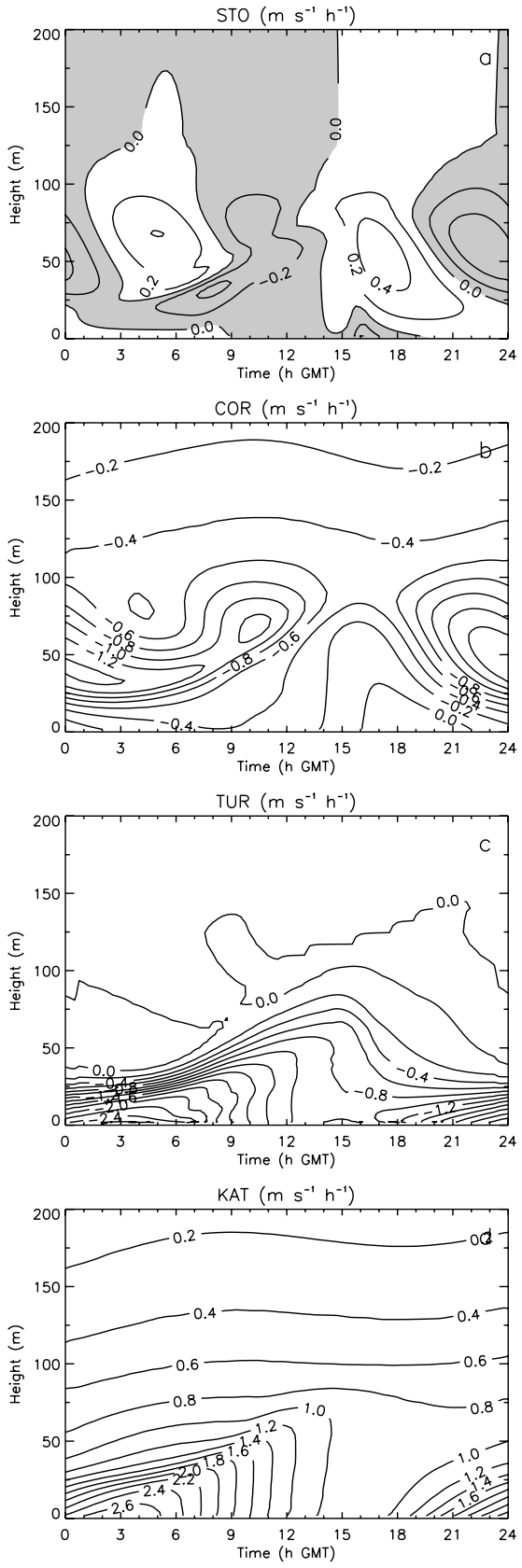

Figure 7. Mean modeled along-slope momentum budget components: (a) storage, (b) Coriolis forcing, (c) turbulent diffusion, and (d) katabatic forcing.

allows more than one full oscillation in the nighttime residual layer, i.e., multiple wind maxima, and is therefore more easily detectable. Second, Figure 7d shows that the katabatic term is nonzero, which complicates the solution above. However, for a katabatic forcing constant in time, which is a reasonable approximation in the residual layer (Figure 7d), and for cos $\beta \approx 1$, which is valid for the Antarctic Plateau, the solution of the two momentum equations is a similar inertial oscillation. In this coordinate system we find an oscillation about the reference wind vector,

$$\overrightarrow{U}_{ref} = \left(u_g + \frac{g}{f} \frac{\theta - \theta_0}{\theta_0} \sin\beta,\ v_g \right). \tag{5}$$

Whereas the direction of a jet due to an inertial oscillation over a horizontal surface is controlled by geostrophic winds [*Blackadar*, 1957; *Andreas et al.*, 2000], over a sloping surface it is also influenced by local topography. For a katabatic forcing and a cross-slope wind speed of the same sign this vector is super-geostrophic. At 70 m height the katabatic forcing is $\sim$0.9 m s^{-1} h^{-1} in our simulation, which implies $\overrightarrow{U}_{ref}$ = (−1.8,4.5). This agrees well with Figure 10 and validates the above assumption of constant katabatic forcing in the residual layer.

[51] To be able to separate the effects of the inertial oscillation from katabatically forced wind, Figure 11 shows the ABL wind speed simulated over a horizontal surface. Over a nonsloping surface, a low-level jet has to be attributed to an inertial oscillation. The result is similar to Figure 1d, implying approximately similar ABL dynamics as with a slope of 1.3 m km^{-1}. A difference is that wind speed is higher in the entire ABL over the sloping surface, especially in the temperature-deficit layer where KAT is largest. In contrast to an ABL dominated by KAT, the low-level jet in Figure 11 decelerates from 2100 GMT onward, though it remains super-geostrophic. From this result, it is clear that katabatic-like wind profiles can be produced by an inertial oscillation, and that caution has to be taken in the interpretation of low-level jets over mildly sloping snow surfaces.

[52] It is not straightforward to recognize an inertial oscillation in the ENABLE observations. Figure 12 shows one night of tethersonde observations by tethersonde during ENABLE in which a possible inertial oscillation is present. The estimated height and time of the wind speed maxima and minima caused by the oscillation are indicated by ''max'' and ''min,'' respectively. The oscillation is less clear than in the model results (Figure 1d). Tethersonde measurements were performed every 3 hours, so they may lack the temporal resolution needed to detect an oscillation of 12.4 hours. Also, in the model simulation we assume a constant geostrophic wind speed and direction. However, these conditions were not entirely met during the simulation period (section 2). In reality, the time-dependent advection of momentum introduces additional variability in strength, phase and period of the measured oscillation, and complicates its detection. A close resemblance to the modeled wind speed dynamics was observed at Mizuho station (70°42′S,44°20′E) in the escarpment region of East Antarctica. *Chiba and Kobayashi* [1986] state that the observed

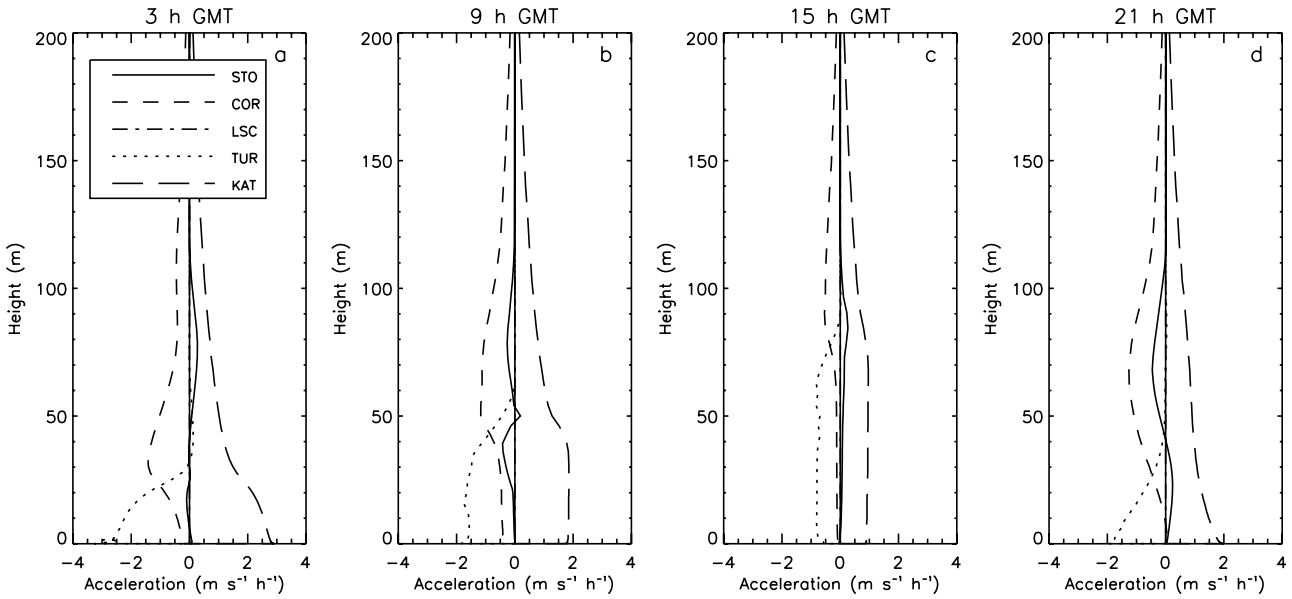

Figure 8. Mean modeled along-slope momentum budget components at (a) 0300, (b) 0900, (c) 1500, and (d) 2100 GMT.

variations in height of the low-level jet are related to both inertial oscillations and subsidence.

5. Summary

[53] We have described the budgets of heat, moisture and momentum of the ABL over the interior plateau of Antarctica for a clear-sky and fair-weather period in summer. For this we used a one-dimensional ABL model which was validated and initiated by measurements made during the EPICA-Netherlands Atmospheric Boundary Layer Experiment (ENABLE) [*van As et al.*, 2006].

[54] A shallow and dynamic atmospheric boundary layer is found. During the night a stably stratified layer of less than 50 m depth with a significant temperature deficit causes saturation of the air and a low-level jet, which persisted up to noon. During the day, surface heating by solar radiation causes a mixed layer that deepens up to 70 m. This reduces the temperature deficit, and also relative humidity and wind speed. The budgets of heat and moisture are dominated by turbulent diffusion. Vertical advection of heat and moisture is relatively small within the boundary layer, but is important above it. Radiative heating or cooling is important near large temperature and humidity gradients, i.e., in the stably stratified layer at night. This component is also relatively large above the atmospheric boundary layer. In the model, moisture is removed by clear-sky precipitation where saturation occurs, mainly in the stable layer between 2000 GMT and the late morning.

[55] Katabatic forcing is largest in the nighttime stable layer, where it is chiefly balanced by turbulent diffusion. Just above the boundary layer, where a small temperature deficit is present owing to radiative cooling, it is balanced by Coriolis forcing. The sudden reduction of friction in the mixed layer at the end of the afternoon triggers an inertial oscillation which causes alternating wind speed minima and

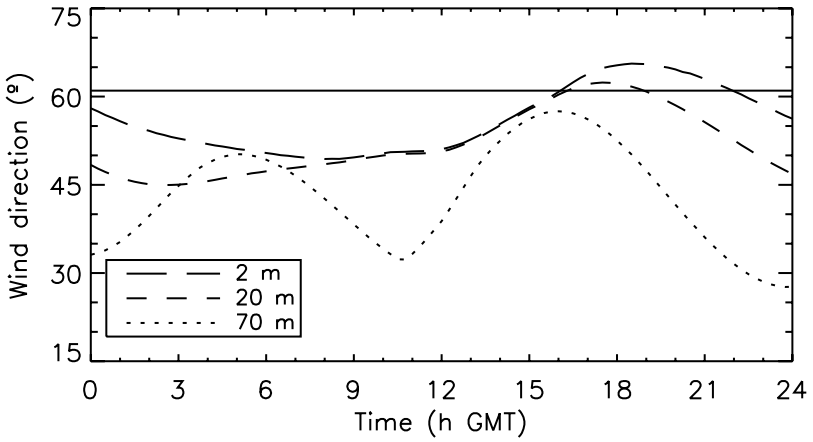

Figure 9. Mean modeled daily cycle of the wind direction at 2 m (long-dashed line), 20 m (short-dashed line), and 70 m height (dotted line).

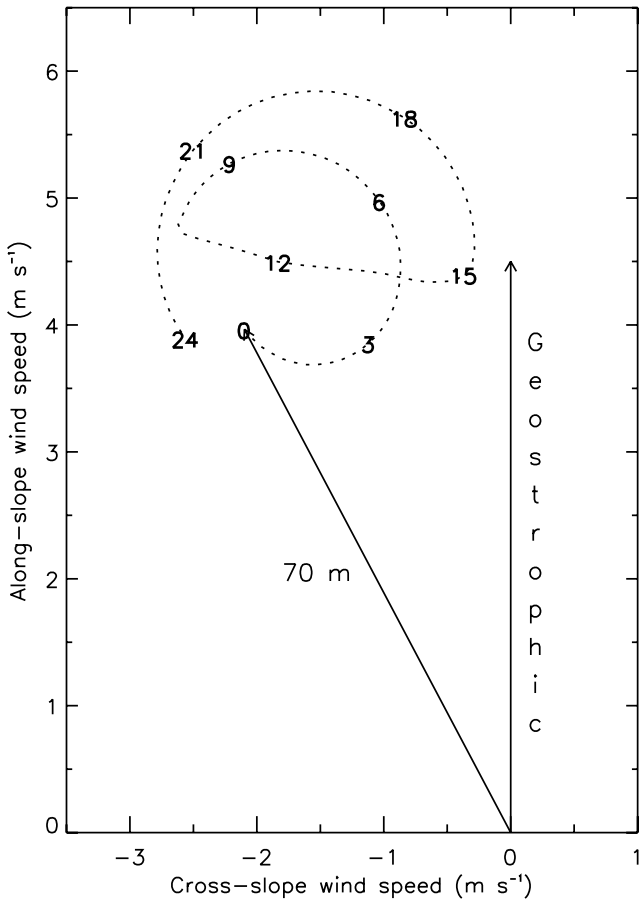

Figure 10. Mean modeled daily cycle of the wind vector at 70 m height. Wind vector for 0000 GMT is given. Numbers indicate time of day in hours GMT. Positive along-slope wind speeds indicate downslope winds.

maxima in the nighttime residual layer. The oscillation is about a vector which is rotated to the left relative to the geostrophic wind, owing to the nonzero katabatic forcing. Similar wind speed dynamics are modeled over a horizontal surface, so caution has to be taken in the attribution of low-level jets over the Antarctic Plateau.

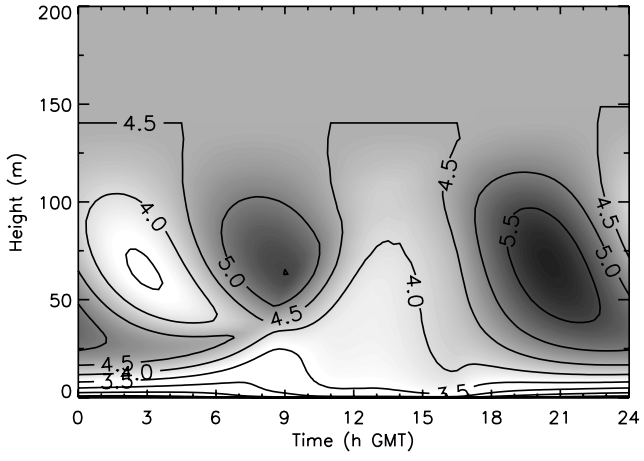

Figure 11. Mean modeled daily cycle of wind speed over a horizontal surface.

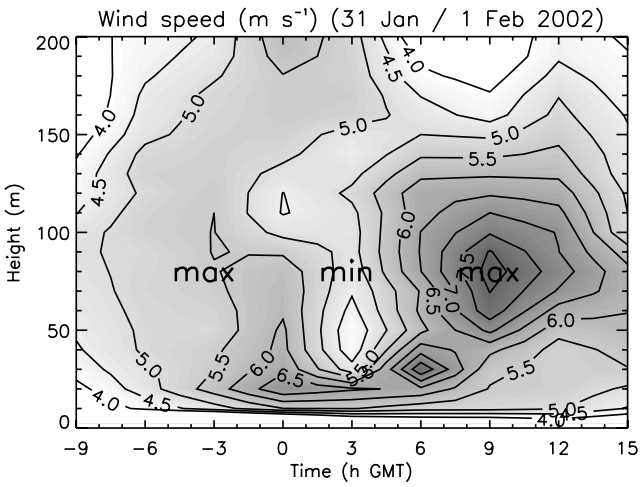

Figure 12. Three-hourly wind speed observations by tethersonde at Kohnen base between 1500 GMT 31 January and 1500 GMT 1 February 2002.

[56] **Acknowledgments.** This paper is dedicated to the memory of Peter Duynkerke. This work is a contribution to the "European Project for Ice Coring in Antarctica" (EPICA), a joint ESF (European Science Foundation)/EC scientific programme, funded by the European Commission and by national contributions from Belgium, Denmark, France, Germany, Italy, the Netherlands, Norway, Sweden, Switzerland, and the United Kingdom. This is EPICA publication 150.

References

Andreas, E. L., K. J. Claffy, and A. P. Makshtas (2000), Low-level atmospheric jets and inversions over the western Weddell Sea, *Boundary Layer Meteorol.*, *97*, 459–486.

Andreas, E. L., P. S. Guest, P. O. G. Persson, C. W. Fairall, T. W. Horst, R. E. Moritz, and S. R. Semmer (2002), Near-surface water vapor over polar sea ice is always near saturation, *J. Geophys. Res.*, *107*(C10), 8033, doi:10.1029/2000JC000411.

Ball, F. K. (1956), The theory of strong katabatic winds, *Aust. J. Phys.*, *9*, 373–386.

Bintanja, R. (2000), Mesoscale meteorological conditions in Dronning Maud Land, Antarctica, during summer: A qualitative analysis of forcing mechanisms, *J. Appl. Meteorol.*, *39*, 2348–2370.

Blackadar, A. K. (1957), Boundary layer wind maxima and their significance for the growth of nocturnal inversions, *Bull. Am. Meteorol. Soc.*, *38*(5), 283–290.

Brost, R. A., and J. C. Wyngaard (1978), A model study of the stably stratified planetary boundary layer, *J. Atmos. Sci.*, *35*, 1427–1440.

Chiba, O., and S. Kobayashi (1986), A study of the structure of low-level katabatic winds at Mizuho station, East Antarctica, *Boundary Layer Meteorol.*, *37*, 343–355.

Deardorff, J. W. (1978), Efficient prediction of ground surface temperature and moisture, with inclusion of a layer of vegetation, *J. Geophys. Res.*, *83*(C4), 1889–1903.

Duynkerke, P. G. (1991), Radiation fog—A comparison of model simulation with detailed observations, *Mon. Weather Rev.*, *119*, 324–341.

Dyer, A. J. (1974), A review of flux-profile relationships, *Boundary Layer Meteorol.*, *7*, 363–372.

Heinemann, G. (1988), On the structure and energy budget of the boundary layer in the vicinity of the Filchner/Ronne ice shelf front (Antarctica), *Beitr. Phys. Atmos.*, *61*(3), 244–258.

King, J. C. (1989), Low-level wind profiles at an Antarctic coastal station, *Antarct. Sci.*, *1*(2), 169–178.

King, J. C., and P. S. Anderson (1999), A humidity climatology for Halley, Antarctica, based on frost-point hygrometer measurements, *Antarct. Sci.*, *11*(1), 100–104.

Kodama, Y., G. Wendler, and N. Ishikawa (1989), The diurnal variation of the boundary layer in summer in Adélie Land, eastern Antarctica, *J. Appl. Meteorol.*, *28*, 16–24.

Kottmeier, C. (1986), Shallow gravity flows over the Ekström ice shelf, *Boundary Layer Meteorol.*, *35*, 1–20.

Lykossov, V. N. (2001), Numerical modelling of interaction between the atmospheric boundary layer and the Antarctic ice shelf, *Russ. J. Num. Anal. Math. Modell.*, *16*(4), 315–330.

Mastrantonio, G., V. Malvestuto, S. Argentini, T. Georgiadis, and A. Viola (1999), Evidence of a convective boundary layer developing on the Antarctic Plateau during the summer, *Meteorol. Atmos. Phys.*, *71*(1–2), 127–132.

Mather, K. B., and G. S. Miller (1967), Notes on topographic factors affecting the surface wind in Antarctica, with special reference to katabatic winds and bibliography, report, 125 pp., Univ. of Alaska, Fairbanks.

Nieuwstadt, F. T. M. (1984), The turbulent structure of the stable, nocturnal boundary layer, *J. Atmos. Sci.*, *41*, 2202–2216.

Parish, T. R., and J. J. Cassano (2003), Diagnosis of the katabatic wind influence on the wintertime Antarctic surface wind field from numerical simulations, *Mon. Weather Rev.*, *131*, 1128–1139.

Parish, T. R., and K. T. Waight (1987), The forcing of Antarctic katabatic winds, *Mon. Weather Rev.*, *115*, 2214–2226.

Parish, T. R., P. Pettré, and G. Wendler (1993), A numerical study of the diurnal variation of the Adelie Land katabatic wind regime, *J. Geophys. Res.*, *98*(D7), 12,933–12,947.

Renfrew, I. A. (2004), The dynamics of idealized katabatic flow over a moderate slope and ice shelf, *Q. J. R. Meteorol. Soc.*, *130*(598), 1023–1045.

Sorbjan, Z., Y. Kodama, and G. Wendler (1986), Observational study of the atmospheric boundary layer over Antarctica, *J. Clim. Appl. Meteorol.*, *25*, 641–651.

van As, D., M. R. van den Broeke, C. H. Reijmer, and R. S. W. van de Wal (2005a), The summer surface energy balance on the high Antarctic Plateau, *Boundary Layer Meteorol.*, *115*(2), 289–317, doi:10.1007/s10546-004-4631-1.

van As, D., M. R. van den Broeke, and R. S. W. van de Wal (2005b), Daily cycle of the surface layer and energy balance on the high Antarctic Plateau, *Antarct. Sci.*, *17*(1), 121–133.

van As, D., M. R. van den Broeke, and M. M. Helsen (2006), Structure and dynamics of the summertime atmospheric boundary layer over the Antarctic Plateau: 1. Measurements and model validation, *J. Geophys. Res.*, *111*, D07102, doi:10.1029/2005JD005948.

van den Broeke, M. R., and N. P. M. van Lipzig (2003), Factors controlling the near-surface wind field in Antarctica, *Mon. Weather Rev.*, *131*, 733–743.

van den Broeke, M. R., N. P. M. van Lipzig, and E. van Meijgaard (2002), Momentum budget of the East Antarctic atmospheric boundary layer: Results of a regional climate model, *J. Atmos. Sci.*, *59*, 3117–3129.

van Lipzig, N. P. M., J. Turner, and M. R. van den Broeke (2004), The near-surface wind field over the Antarctic continent, *Int. J. Climatol.*, *24*(15), 1973–1982.

D. van As and M. R. van den Broeke, Institute for Marine and Atmospheric Research Utrecht (IMAU), Utrecht University, PO Box 80000, NL-3508 TA, Utrecht, Netherlands. (d.vanas@phys.uu.nl)